INSTITUTE OF PHYSICS PUBLISHING MODELLING AND SIMULATION IN MATERIALS SCIENCE AND ENGINEERING

Modelling Simul. Mater. Sci. Eng. **14** (2006) 157–178 doi:10.1088/0965-0393/14/2/003

Molecular dynamics simulations of polymer viscoelasticity: effect of the loading conditions and creep behaviour

Ricardo Simões[1,2], **António M Cunha**[1] **and Witold Brostow**[3,4]

[1] Institute for Polymers and Composites (IPC), Department of Polymer Engineering, University of Minho, 4800-058 Guimarães, Portugal
[2] School of Technology, Polytechnic Institute of Cavado and Ave (IPCA), 4750-117 Barcelos, Portugal
[3] Laboratory of Advanced Polymers and Optimized Materials (LAPOM), University of North Texas, Denton, TX 76203-5310, USA
[4] College of Mechanics and Robotics, AGH University of Science and Technology, Adama Mickiewicza 30, 30-059 Cracow, Poland

E-mail: rsimoes@dep.uminho.pt, rsimoes@ipca.pt, amcunha@dep.uminho.pt and brostow@unt.edu

Received 7 November 2005, in final form 8 November 2005
Published 24 January 2006
Online at stacks.iop.org/MSMSE/14/157

Abstract

Deformation brings out important features of viscoelastic behaviour in polymers. To achieve a better understanding of the underlying phenomena, molecular dynamics simulations have been performed for one- and two-phase polymeric materials created on the computer. An external force was applied to the materials and their response followed as a function of time.

The mechanical properties were found to be strongly affected by the loading conditions, particularly the force increase rate. The simulated materials exhibit a realistic response: the behaviour is more rigid and brittle when the force increases at a higher rate. The material is able to partially recover in a viscoelastic manner if the force is removed after deformation. There are both *quantitative* and *qualitative* differences between the engineering stress and true stress. The presence of a rigid phase in polymer liquid crystals (PLCs) significantly influences their mechanical properties. Higher liquid crystalline (LC) phase concentrations increase stiffness while they make the polymer more brittle. The viscoelastic phase shift is smaller in PLCs than in one-phase amorphous polymers; the LC-rich islands in the LC-poor matrix make the material more elastic.

When a creep force is applied for some time and then removed, the material exhibits partial viscoelastic recovery. The extent of that recovery is dependent on the magnitude of the creep force; a higher applied force results in less recovery. It also depends on the time during which the force was applied; longer times will result in less recovery. These results could be expected,

confirming the model's validity. Unexpectedly the deformation mechanisms at higher stress levels were found to be different from those taking place at lower force levels. This reflects on a more localized deformation for higher creep force levels.

(Some figures in this article are in colour only in the electronic version)

Nomenclature

List of symbols and abbreviations:

MD	Molecular dynamics
CGM	Computer-generated material
t	Number of simulation steps
LC	Liquid-crystalline
PLC	Polymer liquid crystal
f_c	Fraction of flexible bonds in the long conformation state
$\dot{F}$	Force increase rate
I_{F-t}	Integral of the force–time curve
E_{app}	Apparent modulus
E_{sec}	Secant modulus
ε	Strain
σ_n	Engineering stress
σ_t	True stress
δ	Relative peak shift

1. Introduction

Computer simulations have been used to study the behaviour of polymeric materials under external tensile loads. The present paper addresses the viscoelastic phenomena associated with large-scale deformation of these materials. Coarse-grain simulations allow the study of polymeric materials at a mesoscopic level, where the behaviour of individual macromolecular chains can be followed as they respond to the applied load.

Mechanical properties and the performance of polymers and polymer-based systems are a relevant topic for both the scientific community and the manufacturing industry [1]. However, the properties of polymers can be difficult to characterize or to predict due to their complex structure and a variety of factors that influence the material mechanical behaviour—thermomechanical processing history, time-dependent behaviour, anisotropy, etc.

The viscoelastic nature of polymers is a major factor in determining their properties. Although experimental techniques have been employed for many years in the study of viscoelasticity, molecular-level phenomena are far from sufficiently understood. The present simulations aim at providing necessary insights.

Molecular dynamics (MD) is the most widely used method for the simulation of materials. It has been extensively employed to study phenomena which cannot be followed experimentally or to complement information resulting from experiments. A more detailed explanation of the MD method is provided in section 2. As argued by Fossey [2], computer simulations present several advantages, including evaluation of the material response under ideal or hypothetical conditions and also investigating the effect of variables independently of one another.

Other methods of choice within the field of polymer simulations are (a) the Monte Carlo method, which has been employed mostly at the atomistic level [3]; (b) the kinetic model of fracture, used by Termonia and Smith to study the mechanical behaviour of polymers [4, 5] and simulate spider dragline silk [6]; (c) fracture mechanics, used, for example, by Binienda and co-workers to study cracks [7, 8] and reviewed by Nishioka [9]. The various simulation methods were described in detail by Fossey [2], together with examples of their applications.

Among many other topics, MD methods have been used to investigate diffusion and permeation [10, 11], x-ray scattering [12], friction [13] and spider silk elasticity [14]. A MD study of polymer-forming rigid molecules was presented by Farmer and his colleagues [15]. While the molecules investigated are generally recognized as rigid, changes in the end-to-end distances as large as 16% have been found. The simulation results of Farmer provide an explanation for the previously not understood short persistence lengths in solutions and also for some electron micrographs. The mechanical and thermal properties of polyimide nanocomposites have been simulated by Qi *et al* [16], showing that the reinforcing carbon nanotubes increase the material's ability to resist deformation and reduce the softening effect of an increase in temperature.

More relevant to the topic of this paper is the use of MD to study viscoelasticity in polymers and polymer-based materials. The problem of entanglements in viscoelastic polymer *melts* has been addressed by several authors [17, 18]. Polymers containing nanoparticles have also been studied [19]. However, most simulations concerning viscoelasticity deal with solutions and fluids [20–22]. Kroger and co-workers have reported on MD simulations of polymeric fluids and melts in order to study the viscoelastic flow in complex geometries [23] and the effect of the alignment of chain ends on the viscoelastic properties [24].

The state of the art in computer simulations of polymeric materials includes work by Grest on poly(dimethylsiloxane) [25, 26], which exhibits excellent agreement with x-ray scattering measurements. Auhl and co-workers investigated different methods for equilibrating long chain polymer melts [27]. Rottler and Robbins have studied shear yielding in glassy polymers under triaxial loading [28], as well as the growth and failure of crazes in amorphous glassy polymers [29, 30]. Five papers pertaining to recent advances in modelling of polymers by different authors were collected in a special section by Davies (see editorial note [31]).

Creep is a mechanical response of a material characterized by a time-dependent strain increase as a result of the action of a constant applied load. It is a phenomenon which manifests itself in a wide variety of circumstances, including, for instance, the spreading of asphalt in Earth's gravitational field. In polymers, creep may occur readily at ambient or moderate temperatures and cause premature failure of a part—even at stress levels well below the expected material strength. In fact, creep is an interesting viscoelastic evidence of enormous engineering importance; the design of plastic parts should take creep into account if the service involves imposition of loads for relatively long times.

There is no generally accepted method for measuring creep. A method for evaluating flexural creep is described in the ASTM D674 standard. Although used frequently, that standard amounts to a series of recommended experimental practices and precautions to be taken when using creep data. Experimental creep measurements are often made over a long period of time—several months to a year or more. This in spite of the fact that long-term values can be well predicted from relatively short-term tests using the concept of the chain relaxation capability (CRC); see chapter 5 in [1]. Thus, creep for a multiphase polymer liquid crystal (PLC) was predicted for 17 decades on the basis of one-hour tests using an equation for the temperature shift factor a_T derived from the CRC concept [32].

While creep is so prevalent in polymers, it appears also in other classes of materials including metals. Therefore, modelling of creep has been done for metals and

metal-matrix composites, using either viscoelastic models [33] or statistical and numeric approaches [34–36]. Most of these use the finite-element model to perform numerical simulations of creep, and are thus restricted to the capabilities of the continuum approach. Creep in SiC and glass-fibre reinforced polymer-based composites has also been studied using the continuum numeric [37, 38] and damage mechanics [39] models. Some attempts have also been made using MD [40] to study creep in polycrystalline microstructures.

The present work encompasses both amorphous polymers and PLCs, which are typically copolymers containing rigid LC sequences combined with flexible sequences [41]. Thus, PLCs can also be defined as molecular composites; in contrast to heterogeneous composites (HCs), the rigid reinforcing units here are connected to flexible units (chain sequences) by primary chemical bonds. This feature results in a series of improved properties [42, 43]. However, their complexity limits the potential creation of improved PLCs, even though they have been studied using statistical mechanics [44], viscoelastic models [32, 45] and experimental methods [41–43]. Results from computer simulations might provide information needed to establish comprehensive relations between the structure and properties of these materials.

The present paper is a continuation of previous work in the field. Early work concerned the stress relaxation phenomena in both metals and polymers [46, 47]. After that the mechanical properties [48] and the crack formation and propagation phenomena in PLCs [49] were investigated. Key issues here are 'where cracks form' and 'how they propagate'. These could have been expected to appear in the flexible matrix which is relatively weak or in the reinforcing phase which is relatively rigid. Simulations have shown that cracks appear preferentially near the second-phase agglomerates in close proximity and grow along the flexible/rigid interface.

Computer simulations were also employed to study the tribological properties of polymeric materials [50]. Recent work focused on the molecular deformation mechanisms taking place in amorphous polymers and PLCs [51], confirming that the deformation mechanisms are mainly determined by the local chain structure, the presence of chain entanglements and the second phase spatial distribution. The morphology of the material, such as the skin-core ratio in injection moulded parts, was also shown to affect its properties [52].

As mentioned above, it is important to understand that computer simulations are performed to *complement* experimental testing, *not* to replace it. The concomitant use of both methods, together with theoretical approaches, should yield a synergetic effect which will enable the creation of new knowledge-based advanced materials.

2. Simulation model

The amorphous polymer chains are represented by the statistical segment model, as advocated by Flory [53], in which several repeating units of a chain are treated as a single statistical segment. This model is often labelled a *coarse grain* model and allows for simulations at a larger scale than those using the united-atom model or those performed at the atomistic level. The creation of the polymeric materials on the computer is discussed in section 3.

Pair-wise interactions are defined for the segments based on their nature (flexible or rigid) and the type of interaction (primary or secondary). The interaction potentials are defined as a function of the inter-segmental distance. As both one- and two-phase materials were considered, it was necessary to define 4 interaction potentials.

The primary (intra-chain) bonds between rigid LC segments are described by a steep Morse-like potential, significantly limiting the bond extension, and thus, their mobility; see equation (1). The primary (intra-chain) bonds between flexible segments are described by a spliced double-well potential that allows for a change in bond conformation which may occur in real polymer chains; see equation (2). Much weaker secondary (inter-chain)

Table 1. Values of different interaction potentials parameters.

Parameter	Value	Unit
γ_r	10	$(\text{Length})^{-1}$
γ_f	2	$(\text{Length})^{-1}$
U_0	0.05	Energy
Δ	0.732	Length

interactions are described by Morse-like potentials with a relatively broad well, with a smoothed cut-off radius at 2.5σ, where σ is the equilibrium inter-segmental distance. Interactions between unlike segments are always treated as rigid. The potentials were chosen so that the amorphous chains behave as above T_g (the glass transition temperature), with a viscoelastic character.

$$U_r(R) = \{1 - e^{(\gamma_r(1-R))}\}^2 \tag{1}$$

$$U_f(R) = \begin{cases} \{1 - e^{[\gamma_f(1-R)]}\}^2, & R \leqslant 1 \\ 8U_0[(1-R)/\Delta]^2, & 1 < R \leqslant 1 + 0.25\Delta \\ U_0\{1 - 8[1 + 0.5\Delta - R)/\Delta]^2\}, & 1 + 0.25\Delta < R \leqslant 1 + 0.75\Delta \\ 8U_0[(1 + \Delta - R)/\Delta]^2, & 1 + 0.75\Delta < R \leqslant 1 + \Delta \\ \{1 - e^{[\gamma_f(1+\Delta-R)]}\}^2, & R > 1 + \Delta \end{cases} \tag{2}$$

In equations (1) and (2), R is the intersegmental distance, U_0 is the energy barrier for a conformational transition, Δ is the distance between potential wells in flexible bonds and γ_r and γ_f, respectively, define the width of the well for the rigid and flexible bonds. Their values are provided in table 1.

The MD method has been employed in the simulation of the time-dependent behaviour of the system. A leap-frog algorithm [54] was implemented to calculate the time evolution. Reasons for the choice of MD over Monte Carlo or Brownian dynamics methods have been formulated before [48, 49].

The MD method was first introduced by Alder and Wainwright to study the phase diagram of a system comprising hard spheres [55]. Continuous interaction potentials were later introduced in order to obtain a better representation of the forces in physical systems. The next major progress was made by Rahman, who implemented a realistic potential for liquid argon [56], establishing the foundation for the majority of the MD work done since then.

During the simulation, each particle in the system (statistical segments in this case) is characterized by three Cartesian coordinates and three momentum components along the main axes. At every time step of the simulation, these variables are recalculated to provide the evolution in time. In the MD method, time is an explicit variable, allowing for all particles to be moved simultaneously at each time step—this is in contrast to the traditional MC approaches. MD thus allows for the calculation of time-dependent properties, a particularly important feature when dealing with viscoelastic materials.

Throughout this paper time is measured in simulation steps, since the status of the material is not recorded at every time step but only at every 2000 time steps. Thus, each simulation step corresponds to 2000 time steps. For using the MD simulation method, the forces acting on the particles are assumed to be nearly constant over very short periods; this defines the time step for the simulation. In the limit of short time steps it can be shown that this procedure samples states accessible in the micro-canonical ensemble, which implies maintaining the number of particles, volume and energy (NVE) constant throughout the simulation. Additional features

can be added to the algorithm in order to specify the configurational temperature, or allow the simulation to access a range of energies and/or pressures that correspond to either the canonical or the isothermal–isobaric ensembles.

The simulations reported in the present paper were performed at a constant (room) temperature in order to avoid the effect of stochastic thermal forces, since the purpose is to study non-thermal sources of polymer fracture [47]. Thus, the simulations were carried out in the isothermal ensemble (NVT), with the constant temperature maintained by coupling the system to an external bath, using what is often termed the *Berendsen thermostat* [54].

Before the simulation begins, the segments are disturbed from their initial lattice-based positions by a small random value (less than 1% of the equilibrium intersegmental distance). At the first stage of the simulation the material is allowed to equilibrate for 2000 time steps without any external forces being applied. The perturbation from the ideal lattice positions, followed by equilibration, results in a starting configuration appropriate for the off-lattice simulation. The 2000 time steps were found adequate for the material to recover from the induced perturbation; after this period the segments are merely oscillating near equilibrium distances. When the quasi-equilibrium state has been reached, a uniaxial external tensile force is applied to the edges of the material. For the simulations reported in the present paper, the force is applied along the x-axis. The state of the system is monitored and recorded periodically. The value of the external force can be controlled at each time step, as described in section 4.1. The previous work had focused on large-scale deformation up to fracture under a continuously increasing tensile force [49]. The results of the present paper were obtained under an external force increasing from an initial value of zero up to a pre-determined value and then decreasing at the same rate.

Uniaxial extension constitutes the most widely used mechanical test. At each instant, the *engineering stress* (σ_n) is calculated as the ratio of the applied tensile force to the initial cross-sectional area, $\sigma_n = F/A_0$. However, during that extension the minimal cross-sectional area (A_m) of the specimen decreases compared with the value measured before force application. The true stress (σ_t) takes into account the change in time of the minimal cross-sectional area, $\sigma_\mathrm{t} = F/A_\mathrm{m}$. Failure of the specimen occurs earlier than the engineering stress values would suggest. As the present simulations have the capability to evaluate both kinds of stress, the differences between them are presented and discussed below.

Recently, a procedure for calculating true stress in computer-generated materials (CGMs) has been proposed [57]. The CGM is divided into 10 parallelepiped sections of equal length along the x-axis (the number of sections could easily be increased if a more detailed analysis was required); see figure 1(*b*). The geometry of each section is described by the position of the eight segments at its corners. These corner segments are assigned to their respective sections at the beginning of the simulation and their position tracked in time.

Each section can thus be characterized by two cross-sectional areas: a left cross-sectional area defined by the leftmost segments (A_l) and a right cross-sectional area defined by the rightmost segments (A_r); see figure 1(*b*). The cross-sectional area of the section (on the y–z plane) is simply the average of A_l and A_r. True stress σ_t can then be calculated at each time step based on the cross-sectional area. By definition, the highest value of σ_t found in any section is the true stress in the specimen; see equation (3).

$$\sigma_\mathrm{t} = \frac{F_\mathrm{ext}}{\min\{\bar{A}_1, \bar{A}_2, \ldots, \bar{A}_{10}\}}. \tag{3}$$

Due to the non-homogeneous nature of the deformation process, with both localized necking and crack formation occurring under different conditions, the shape of the true stress curve should be quite different from that of the engineering stress. Moreover, abrupt changes

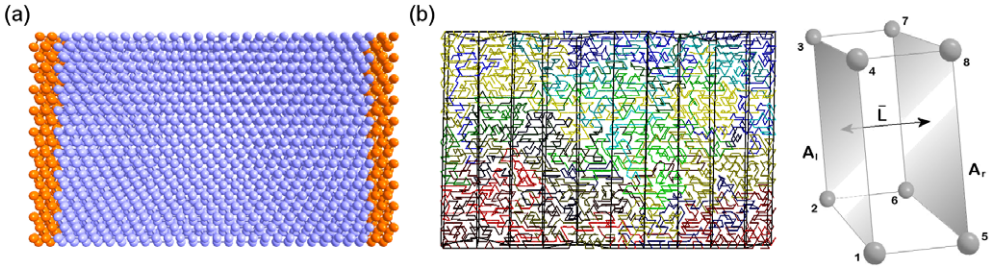

Figure 1. A CGM within a simulation cell containing approximately 1800 segments: (*a*) sphere representation: light spheres represent the flexible segments that constitute the amorphous chains, while dark spheres represent rigid segments which are placed at both edges along the x-axis to prevent chain pullout due to the direct force application on these segments; (*b*) chain representation: division into sections and detail of a section. Note that each chain is represented in a different shade of grey for easier visualization.

in the true stress are often observed, corresponding to the occurrence of specific phenomena at a sufficiently large scale throughout the material (e.g. crack propagation).

It should be clear from this description of the true stress measurement procedure that no periodic boundary conditions are used in the present simulations. Otherwise, it would not be possible to measure the changes in the cross-sectional area as described above.

Some unavoidable approximations are implicit in this analysis: whenever a segment is intersected by the boundary between two sections it is considered as belonging to only one of them, and a very small number of segments sometimes escape the overall boundaries of all sections. These effects have been thoroughly tested and present a negligible effect on the final results. However, when the system reaches large-scale deformation, the shape of the sections may become inadequate for calculating the cross-sectional area. In these cases, the user must determine up to which simulation step the values of the true stress should be considered.

As the present simulations are conducted at the mesoscale, the use of the general concept of macroscopic strain at this scale is arguable. The strain is thus calculated based on the deformation of the sections, that is, from the distance between the leftmost and the rightmost cross-sections of the material (A_l of section 1 and A_r of section 10). The geometry of the sections is also the basis for determining the free volume in the material, although the results pertaining to that analysis will be discussed elsewhere.

It should also be pointed out that as in earlier work [48], a coherent dimensionless system of units is used. The length of a non-strained bond corresponds to a unit of length, the mass of a single statistical segment corresponds to a unit of mass and the energy needed to dissociate a bond corresponds to a unit of energy. All other quantities can be derived from these; for example, a unit of force is given by the ratio of one unit of energy to one unit of length.

Further details concerning the simulation model were previously provided elsewhere [47,48].

3. Material generation procedures

Both one- and two-phase materials were created in order to study amorphous polymers as well as those containing a rigid reinforcement (such as PLCs). In both cases, the amorphous phase consists of coiled chains that exhibit a certain molecular weight distribution. Although the coiled chains can be created with a preferential orientation (or even complete alignment with a specified direction), that feature was not used in these simulations. Thus, the resulting

amorphous phases are always randomly oriented. In the case of PLCs, the rigid LC phase is added to the flexible matrix after the generation of the coiled chains.

The approach followed to generate the amorphous phase is based on a procedure developed by Mom [58] and later modified to exhibit more realistic features [59]. This approach can be used to create both completely filled lattices and those containing vacancies. In the beginning of the procedure, a hexagonal close packed lattice is filled with segments at equidistant positions. This lattice was chosen for reasons previously discussed [46, 59]. In particular, it has a more realistic coordination number than for instance the simple cubic lattice. Each of the statistical segments represents a piece of a polymeric chain, as discussed in section 2.

Before chain growth, each individual segment in the material constitutes a chain of length, l. The system is then searched for neighbouring segments that are available for bonding. In the early stages of the procedure, many pairs of segments will fulfil this condition; in that case, a statistical function determines which segments bond and, if one segment can bond to any of several neighbours, which direction the bond should take. This procedure is repeated and chains continue to grow by the bonding of neighbouring end-of-chain segments until no more segments can be bonded in this way. Additional chain-growth procedures [59] were developed to increase the average chain length and simultaneously introduce vacancies in the material—an important feature for realistic representation of a polymeric material.

In the case of two-phase PLCs, the rigid LC phase was found experimentally to form agglomerates of a quasi-spherical shape, called *islands* [60, 61]. For the generation of PLCs, the flexible matrix is created first, after which the rigid second phase is added in the form of islands. These are introduced by random sequential addition until the desired LC concentration is obtained. A series of CGMs with different LC concentrations were created in order to study the effect of this parameter on the behaviour and properties of the material.

It is important to maintain other parameters constant when investigating effects of the LC concentration. However, due to the random nature of the material generation procedure, each CGM exhibits a different amorphous chain structure. Also, the placement of the LC islands on two-phase PLCs results in random island spatial distributions. Thus, it was necessary to prevent effects caused by changes in these two parameters, as they have been shown to affect the mechanical response [49, 62]. This was achieved by creating a CGM with the highest desired LC concentration and then using it as a template for the creation of lower concentration materials by random removal of islands.

A detailed description of the material generation procedure has been provided elsewhere [59]. An example of a CGM within a cell containing approximately 1800 statistical segments is shown in figure 1(*a*). As mentioned before, the lattice is used only to position the segments and create the initial chain configuration; the simulations were carried out in continuous space.

4. Effect of the loading conditions

The properties of polymers depend on the imposed loading mode and experimental variables, particularly the strain rate. The strain rate-dependent viscoelastic phenomena exhibited by polymers are mostly due to the molecular motions required for deformation. A common problem is the material embrittlement at high loading rates (such as impact). The dependence of the tensile properties on the strain rate has been observed by several authors [63, 64]. To verify this dependence, a series of simulations were performed with varying conditions.

Since the simulations discussed here are not strain-rate controlled but force–rate controlled, the force increase rate, $\dot{F}$, is the variable that determines the loading conditions. In these simulations the force increases at a constant rate up to a maximum value and subsequently

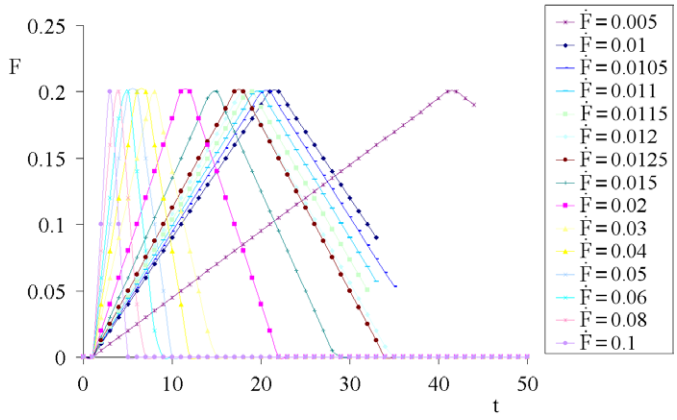

Figure 2. Different force increase rates, $\dot{F}$, used for simulation. Here t is the number of simulation steps and F is the force.

decreases at the same rate. The maximum force value was chosen to induce a significant amount of plastic deformation in the material before the force starts decreasing.

4.1. Loading rate

A single-phase material containing approximately 1800 statistical segments was tested as well as materials of the same dimensions but containing 20% and 30% LC concentration. The results for two-phase materials are discussed in section 4.3. Force increase rates, $\dot{F}$, used for simulation vary between 0.005 and 0.1, as shown in figure 2.

It is clear from figure 2 that in most cases the force returns to zero without the material being fractured. However, for slower rates, *the material fractures while the value of the force decreases*. Two reasons are proposed for explaining this behaviour: (i) slower rates allow more time for molecular deformation mechanisms to develop and (ii) high values of the force are applied for an extended time in slower rates. Fracture can occur during the force decrease stage if the force is still high enough to induce deformation, particularly if the material has already been extensively deformed.

The integral of the force–time curve (I_{F-t}) can be calculated as the area beneath the curve up to the peak:

$$I_{F-t} = \int_0^{t_{\max}} F \, \mathrm{d}t \tag{4}$$

Here $t_{\max}$ corresponds to the time at which the highest external force was applied. The value of I_{F-t} is a measure of the amount of energy provided to the material for deformation. From the analysis of figure 2, the critical $\dot{F}$ that results in fracture can be determined. I_{F-t} can then be plotted as a function of $\dot{F}$ and the critical rate pinpointed. This is shown in figure 3.

In the case of this material, the critical $\dot{F}$ is 0.0115. Any slower rates will result in fracture before the force returns to zero. Note that the critical rate was found by an iterative process, performing simulations between conditions that cause fracture and those that do not. Obviously, this process could continue by performing another simulation for instance with $\dot{F} = 0.011\,75$; however, increased precision in the critical rate would not provide new relevant information.

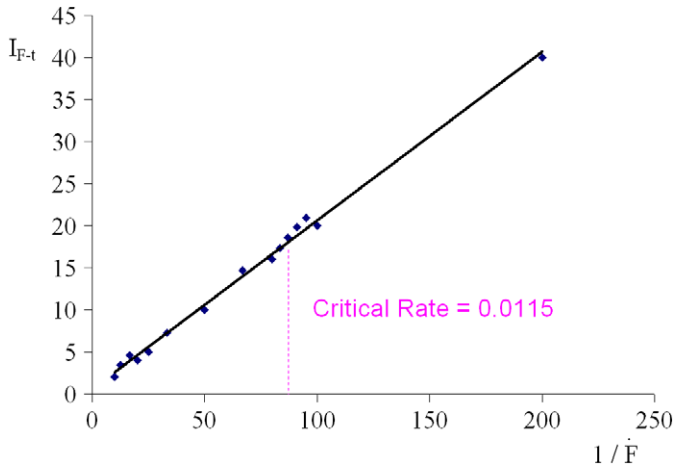

Figure 3. Force–time integral I_{F-t} for the different force increase rates $\dot{F}$.

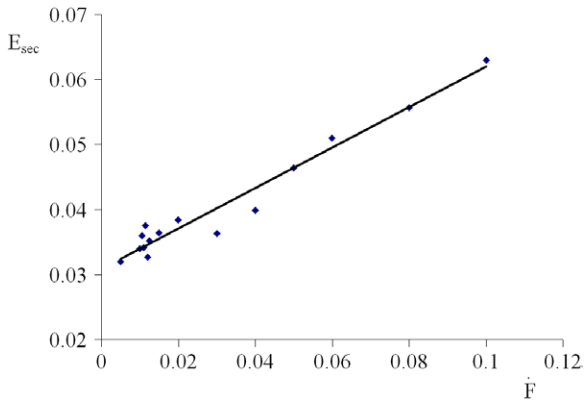

Figure 4. Effect of the force increase rate $\dot{F}$ on the secant modulus E_{sec} of the material.

The material stiffness behaviour was also investigated for different values of $\dot{F}$. The modulus has been calculated using two different methods: (i) the apparent modulus (E_{app}) is determined from the slope of the initial linear region of the stress–strain curve and (ii) the secant modulus (E_{sec}) is determined from the slope of the line connecting the origin to the point on the stress–strain curve at the strain of 0.1. Since E_{app} and E_{sec} behave similarly, the results presented are based on the secant modulus; see figure 4. Although there is some scatter, the clear tendency is for the modulus to increase with an increasing $\dot{F}$, confirming experimental evidence of increased rigidity for higher loading rates.

The material also exhibits different strain behaviour for different loading conditions. Figure 5 clearly distinguishes between rates that result in fracture and those for which recovery is observed. Since many force increase rates were simulated, simultaneously representing all of them significantly reduces legibility of the plots. Thus, several of the figures shown in this paper represent only selected values of $\dot{F}$.

Results show that the higher the rate, the lower the maximum value of the strain. In addition, the strain maximum occurs sooner. This would be expected, since the force was

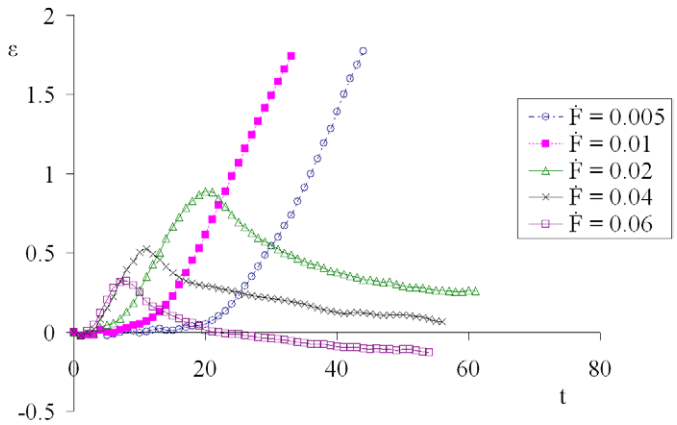

Figure 5. Effect of the force increase rate $\dot{F}$ on the strain ε. Here t is the number of simulation steps.

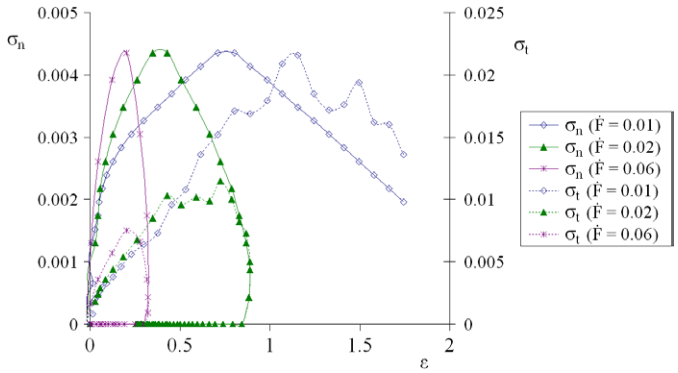

Figure 6. Engineering stress σ_n versus strain ε (left axis, full lines) and true stress σ_t versus strain ε (right axis, dashed lines) behaviour for different force increase rates $\dot{F}$.

applied for a shorter period. However, the curves for different $\dot{F}$ that do not cause fracture are similar in shape. This confirms that the molecular phenomena involved in the different simulations are the same, occurring only at different time frames.

The engineering stress versus strain curves are similar to those of force versus time up to the maximum force values; see figure 6. The viscoelastic recovery in time can also be seen in these stress–strain curves. However, the true stress curves provide important information that the engineering stress curves do not. Figure 6 clearly shows how the maximum true stress level varies significantly for the different $\dot{F}$ values. Also, the true stress keeps *increasing* even after the force starts to decrease. Clearly the force is still sufficient to induce deformation, thus changing the cross-sectional area. For the rate of 0.01, it seems from figure 6 that the true stress was starting to decrease at a point, since the applied force had been significantly reduced; however, the material still fractured.

The force increase rates that do not result in fracture exhibit lower maximum true stress values occurring at lower strains. This is due to the fact that at these higher rates the cross-section does not have time to change significantly. The true stress curves also display a higher slope for higher $\dot{F}$. Thus, if these curves had been used to calculate the modulus, the results would be similar to those represented in figure 4 for the engineering stress.

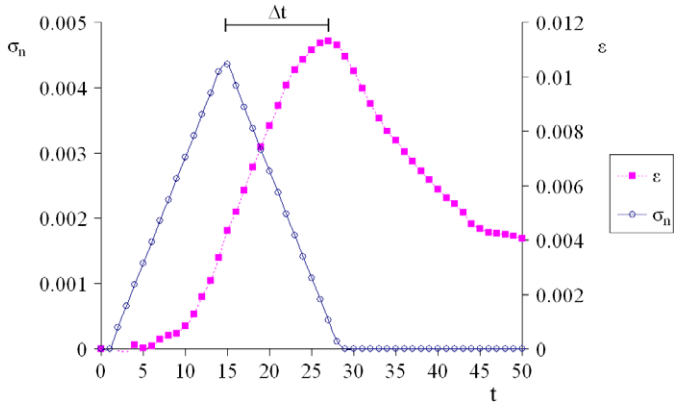

Figure 7. Time shift between the stress σ_n and strain ε peaks. Here t is the number of simulation steps.

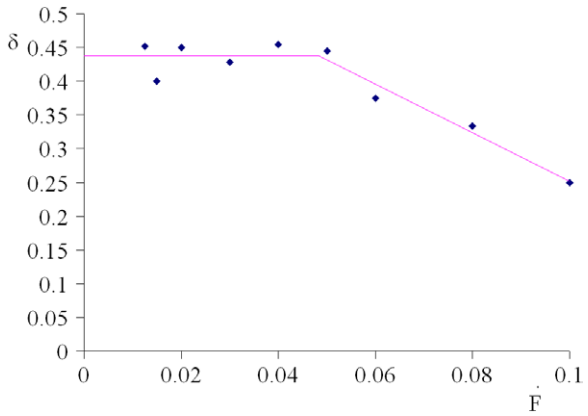

Figure 8. Relative peak shift δ for different force increase rates $\dot{F}$.

4.2. Time-dependent response

There is always a lag between the applied load and the strain response in viscoelastic materials. In dynamic mechanical analysis (DMA) this results in a shift between the stress and strain curves called the *phase angle* [65, 66]. In the simulations, although no oscillating force was used, a lag also appears in the strain response when the force is applied for some time and then removed; see figure 7. The CGM used here is the same as considered in section 4.1.

That lag can be quantified as the relative shift, δ, between the peaks, $\delta = (t_\varepsilon - t_\sigma)/t_\varepsilon$. Here, t_ε and t_σ are, respectively, the times at which the maximum strain peak and the maximum stress peak occur. A shift value of zero implies an ideally elastic material whereas a value of 0.5 would correspond to an ideally viscous (liquid-like) material.

The shift of the engineering stress and strain curves has been calculated for each force increase rate from figure 2. As shown in figure 8, the shift for this material seems to oscillate around a high value for low $\dot{F}$ and then decreases significantly for higher $\dot{F}$. The line marked in figure 8 has two linear regions. The first region at low $\dot{F}$ is the average value of δ for the first five points. The second region is a linear regression for the last four points. This line was drawn for easy visualization of the trend.

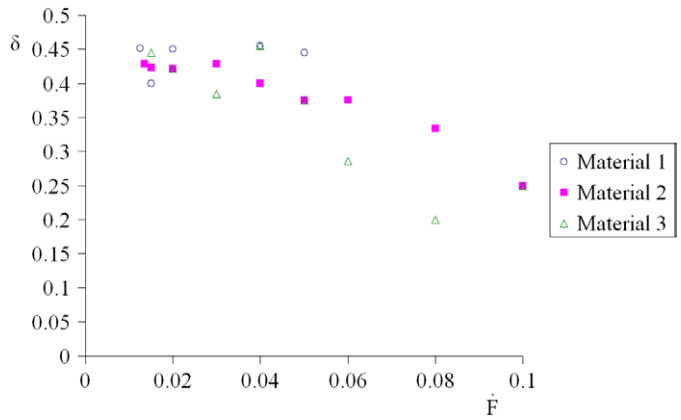

Figure 9. Relative peak shift δ for the simulated materials at different force increase rates $\dot{F}$.

The force increase rate is directly related to the extent of deformation, as noted above. Higher rates result in lower deformation, since the force is applied for a much shorter period. Thus, it is reasonable to expect lower δ values or a more elastic behaviour. For lower $\dot{F}$, there is large-scale plastic deformation, resulting in higher δ; again see figure 8. For rates below 0.05, the shift seems to stabilize around 0.44. Therefore, deformation at low $\dot{F}$ is indeed dominated by the *viscous* component of the material. At high $\dot{F}$, the *elastic* component dominates.

To verify if the shift is independent of the material structure, similar simulations have been performed on another single-phase CGM of randomly oriented chains as well as a two-phase CGM with 30% LC concentration. The results for the three materials are comparatively shown in figure 9.

Although there is some scatter, the behaviour seen for the first material is similar for the other two materials. In fact, for $\dot{F}$ above 0.06, both single-phase materials exhibit exactly the same shift. The two-phase material exhibits overall lower δ values, since the reinforcement makes the material more rigid and simultaneously more elastic. Equal shift values were observed for the three materials at the highest $\dot{F}$, although this effect may be partially due to a very small number of points in the stress and strain curves.

4.3. Second phase concentration

The effect of the force increase rate was investigated in two-phase materials with 20% and 30% LC concentration. This provides an opportunity to study the effect of the second phase concentration on the mechanical properties. The behaviour is similar to that described in section 4.1 for a single-phase material. However, there are differences due to the presence of the LC islands.

The apparent modulus was calculated and compared with the case of the single-phase material; see figure 10. As could be expected from previous arguments, the presence of the LC phase increases the modulus of the material. The tendency of the modulus to increase with increasing $\dot{F}$ is also observed for the two-phase systems. However, it seems that $\dot{F}$ has a higher effect on the modulus than the presence of the second phase, at least in the range of the LC concentrations studied.

The presence of the second phase also influences the strain behaviour. The two-phase materials exhibit delayed response to the applied force since the LC reinforcement increases the rigidity; see figure 11. Thus, for higher LC concentrations, the same strain levels take a

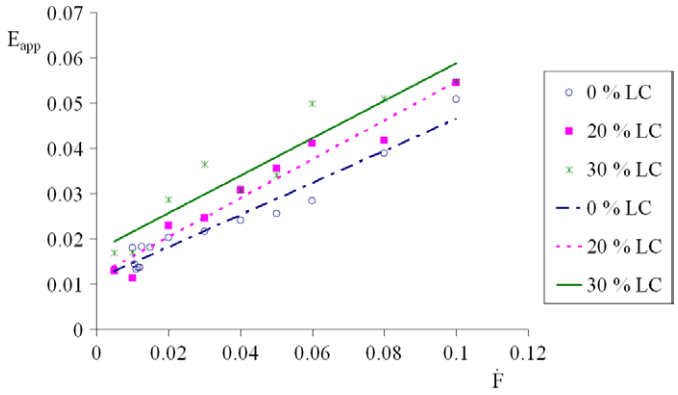

Figure 10. Effect of the LC concentration on the apparent modulus E_{app} of the simulated materials at different force increase rates $\dot{F}$.

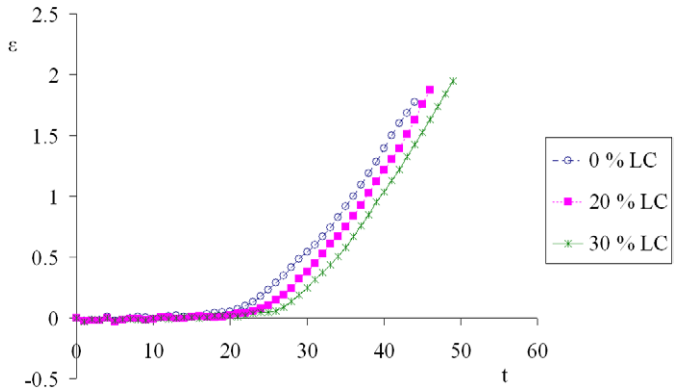

Figure 11. Effect of the LC concentration on the strain ε at the force increase rate of 0.005. Here, t is the number of simulation steps.

longer time to reach. This is equivalent to saying the same strains occur at higher values of the force. Although the curves are displaced in time, their shapes are very similar.

The evolution of engineering and true stress levels during deformation has also been compared. These are shown in figure 12 for a material that is allowed to recover without fracture. Although the two plots look similar, several important differences should be noted. The stress magnitude is quite different; the maximum σ_{t} is almost twice the maximum σ_n. This demonstrates the importance of measuring the cross-sectional area for obtaining accurate stress information. The geometry of these specimens is quite simple. For complex geometries, the difference between σ_n and σ_{t} might be even more drastic. The true stress curves are also slightly slanted compared with the engineering stress curves. These results again show a minor time shift between σ_n and σ_{t}, due to the time-dependent phenomena accompanying changes in the cross-section.

For all cases, the LC phase appears to decrease the strain at which the maximum stress appears, and for σ_{t} the maximum stress value is also decreased. Thus, the LC islands are performing their role as reinforcement.

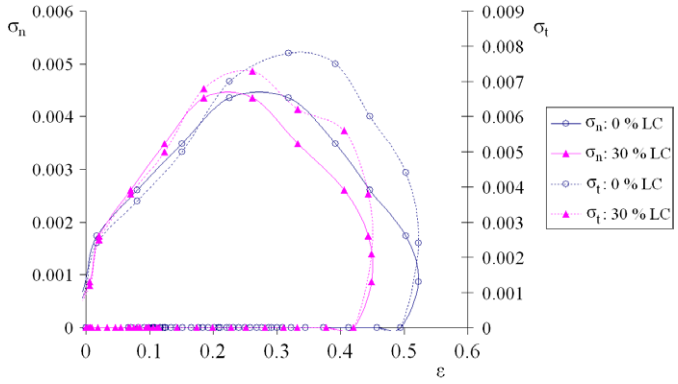

Figure 12. Engineering stress σ_n versus strain ε (left axis, full lines) and true stress σ_t versus strain ε (right axis, dashed lines) at the force increase rate $\dot{F}$ of 0.04.

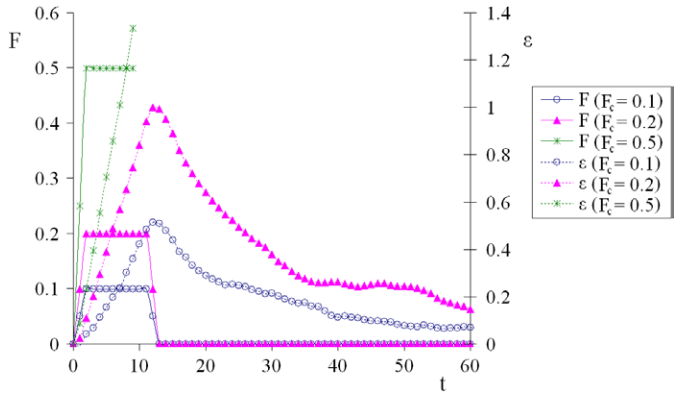

Figure 13. Different creep force patterns used for simulation and the respective strain behaviour of the material for each. Here t is the number of simulation steps, F_c is the creep force and ε is the strain.

5. Creep behaviour

The behaviour of a CGM within a simulation cell containing approximately 1800 statistical segments was simulated under different creep conditions. In section 5.1, the effect of the creep force value on the mechanical response is discussed. In section 5.2, the creep force value was kept constant while the duration of its application was varied. Some of the interesting features observed in the results are discussed further in section 5.3.

5.1. Effects of creep force variation

A constant creep force was applied for 10 simulation steps in each case and then removed. The force application patterns are shown in figure 13. An intermediate step where the force is half the maximum value was introduced between the force of zero and the creep force. As shown in figure 13, at the highest creep force the material fractures after 7 simulation steps. In other cases, the material exhibits partial viscoelastic recovery with time.

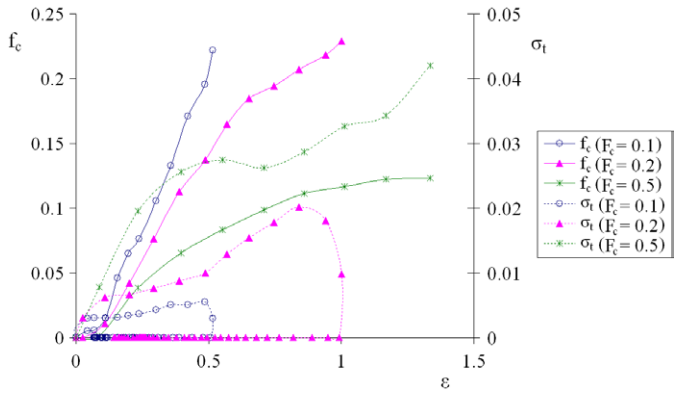

Figure 14. Bond conformation changes (left axis, full lines) and true stress σ_t versus strain ε behaviour (right axis, dashed lines) for varying creep force levels. Here, F_c is the creep force, f_c is the fraction of bonds that have undergone conformational change and ε is the strain.

The strain response in time for each of the force application patterns is also shown in figure 13. For the case of the highest force, the strain increases continuously until fracture occurs. When the force is removed and the material recovers, the behaviour is similar for different force values. However, the strain increases more rapidly for higher force values, as could be expected. Also, higher force values will cause higher maximum strain values. Even at the lowest creep force simulated, the viscoelastic nature of these materials is evident. The creep seen as a continuous increase of the strain at a constant force value reflects the time dependence of the deformation mechanisms.

The simulation model employed allows for short and long bonds, such as those present as *cis* and *trans* in carbonic chains. The differences in the strain response at varying creep forces indicate that different deformation mechanisms are taking place. This can be verified by plotting the fraction of flexible bonds in the long conformation state, f_c, for different conditions; see figure 14. Clearly, the value of f_c provides a measure of the extent of bond conformation changes that the material has undergone.

Thus, the strain increases more rapidly for higher creep force levels. However, that is not due to more bonds undergoing conformational changes. In fact, the force of 0.5 corresponds to the highest strain but results in a much lower number of bonds in the long state than at the other force levels. This implies that other deformation mechanisms are predominant for higher force values. As discussed in more detail in section 5.2, higher forces tend to rapidly cause chain unfolding and chain separation near the edges of the material, while the bulk material is still mostly unchanged. Since f_c is very similar for the lower force values, there might be a critical creep force value that induces this effect.

The true stress (σ_t) profile also varies for different conditions. As shown in figure 14, although applied for the same period of time, higher forces correspond to higher deformations. It could be expected that higher values of the force would result in proportionately higher true stress values. However, the maximum value of the true stress for the force of 0.2 is approximately four times larger than that for the force $= 0.1$. This implies that the cross-section is also changing more significantly for the higher creep force. Thus, the combined effect of the increased external force and the reduced cross-section causes the true stress to reach higher values than expected. In the case of the highest creep force, the true stress was still increasing when fracture occurred.

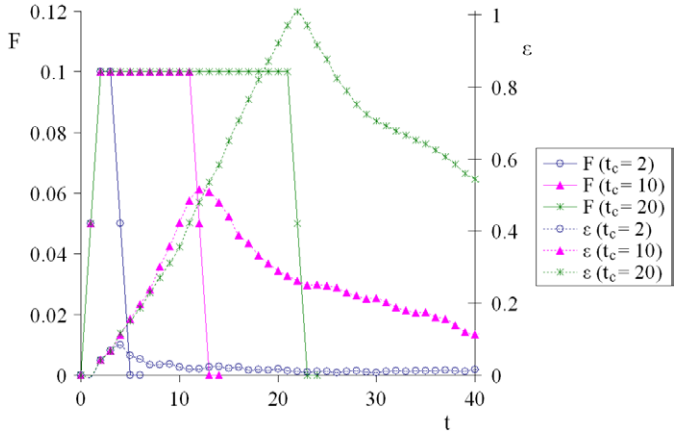

Figure 15. Different creep time patterns at creep force $F_c = 0.1$ (left axis, full lines) and the respective strain behaviour of the material for each (right axis, dashed lines). Here t is the number of simulation steps, t_c is the creep time and ε is the strain.

5.2. Stress imposition time effects

For each level of the creep force described in section 5.1, the creep time, t_c, of the simulation was varied between 2 and 20 simulation steps. Following the argument from the previous section that the molecular phenomena responsible for deformation mechanisms are time dependent, these simulations should exhibit significant differences. A few selected force application patterns for the force level of 0.1 are represented in figure 15.

The strain response in time is also shown in figure 15. The simulation with creep time $t_c = 2$ exhibits only small-scale deformation; when the force is removed, recovery to a state very close to the original shape occurs. In the other simulations with higher creep times, there is large-scale deformation. Thus, the material does not recover to the initial shape; instead, when it recovers, it tends to buckle.

The shape of the curves for $t_c = 10$ and $t_c = 20$ is similar, all involving large-scale deformation and subsequent recovery. As expected, the maximum value of the strain is higher for longer times of creep force application. An interesting feature of the plot is that the curves have very similar shape in the initial overlapping region. This would be expected, since it is the same material under the same loading conditions.

Related features can be seen in the stress–strain diagram; see figure 16. The shape of the curves in the overlapping region is very similar. The maximum true stress in the material increases for increased creep time—which implies a continuous decrease of the cross-sectional area.

The strain response for the force level of 0.2 is shown in figure 17. The main difference with respect to the force level of 0.1 is the fracture of the material after 20 simulation steps at the creep force. The shape of all curves in this figure is identical in the overlapping region, as seen before for the lower force level.

5.3. Strain behaviour

Based on the results for the different creep forces applied for varying t_c, some very interesting properties of this material can be established. As shown in figure 18, the strain after only

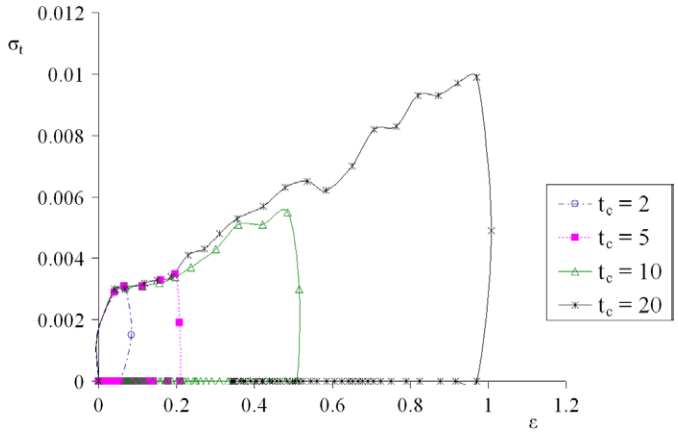

Figure 16. True stress versus strain behaviour for varying creep time at creep force $F_c = 0.1$. Here t_c is the creep time, σ_t is the true stress and ε is the strain.

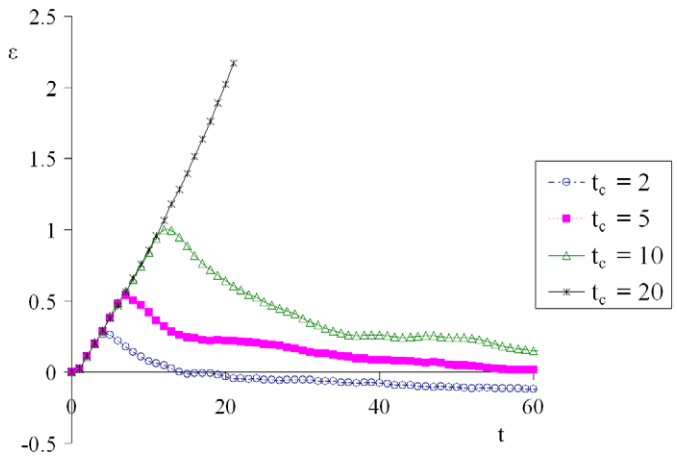

Figure 17. Effect of the creep time on the strain behaviour of the material at creep force $F_c = 0.2$. Here t is the number of simulation steps, t_c is the creep time and ε is the strain.

2 simulation steps at a force of 0.5 is equal to the strain after 5 simulation steps at a lower force of 0.2. The same is observed for the strain after 10 simulation steps at a force of 0.2 and after 20 simulation steps at a force of 0.1.

However, even though they exhibit similar maximum strain, the deformation mechanisms are not the same; apparently, the changes in geometry during deformation are different for each case. Figures 19(*a*) and (*b*) represent the material structure at the last time step of creep force, immediately before the force starts decreasing for the cases of $t_c = 10$ at a force $F = 0.2$ and $t_c = 20$ at a force $F = 0.1$, respectively.

The lower force applied for an extended period of time results in a more homogeneous deformation throughout the material, with most chains having unfolded and extended along the force application direction. For the higher force, which is sufficient to break weak secondary forces, the chains near the edges can unfold rapidly and start extending significantly while the inner material has not yet shown deformation. In this case, the final structure geometry

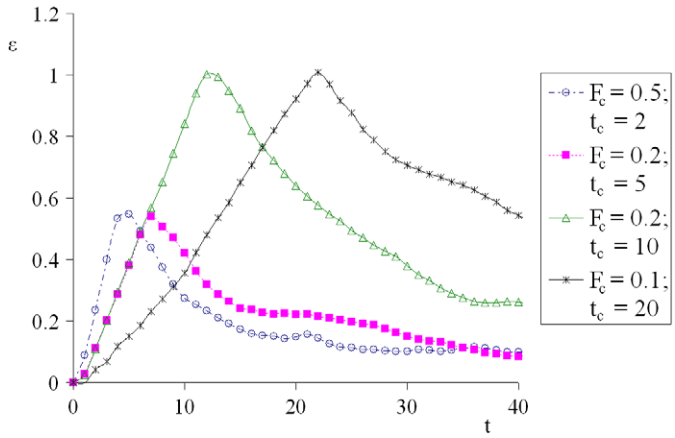

Figure 18. Strain behaviour under varying conditions of creep force and time. Here t is the number of simulation steps, t_c is the creep time, F_c is the creep force and ε is the strain.

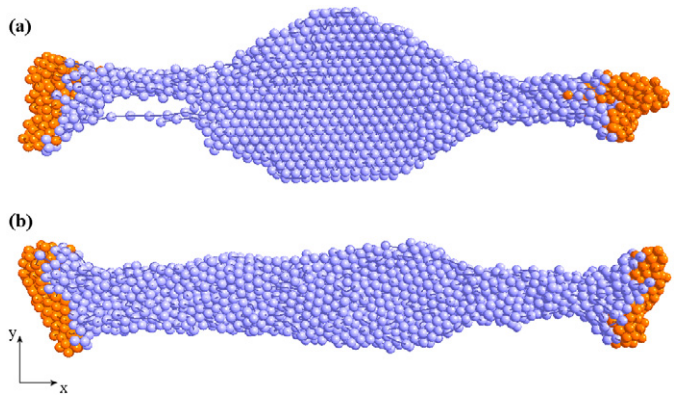

Figure 19. (*a*) Structure of the material before force removal for the case of $t_c = 10$ at a force $F = 0.2$; (*b*) structure of the material before force removal for the case of $t_c = 20$ at a force $F = 0.1$. Light spheres represent the flexible segments that constitute the amorphous chains, while dark spheres represent rigid segments which are placed at both edges along the x-axis to prevent chain pullout due to the direct force application on these segments.

indicates that if the force had not been removed at that particular moment, fracture would occur rapidly. This does not appear to be the case for the lower creep force.

The different deformation mechanisms which have developed in these two cases are reflected in the number of bonds undergoing conformation change; see figure 20. The three creep loading conditions result in similar strain level before force removal. However, higher force results in a lower number of bond conformation changes. Simultaneously, higher force results in a much more localized deformation. This is in agreement with what was argued above regarding the different deformation mechanisms taking place in the material. Strain for higher force values results more from chain separation, even causing cracks to develop at relatively low strain values due to chain pullout. In contrast, lower force values allow the external force to be better distributed through the material, resulting in more chain unfolding accompanied by bond conformation changes.

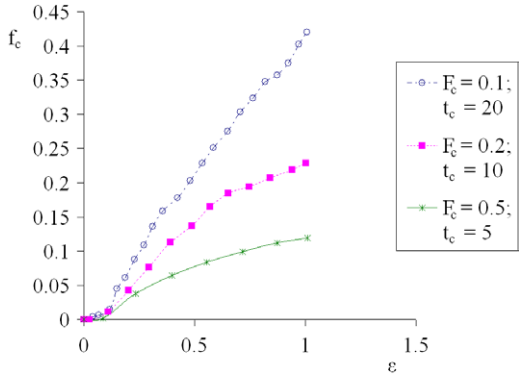

Figure 20. Effect of the creep loading conditions on the bond conformation changes. Here t_c is the creep time, F_c is the creep force, f_c is the fraction of bonds that have undergone conformational change and ε is the strain.

Thus, each of the competing deformation mechanisms observed in the simulations, such as chain unfolding and chain separation, has its own time dependence.

6. Concluding remarks

The loading conditions were found to greatly influence the mechanical properties. As $\dot{F}$ increases, the material becomes stiffer, more brittle and, as can be expected, lower values of the strain at break are found. In terms of the viscoelastic behaviour, for relatively low $\dot{F}$, deformation is dominated by the *viscous* component of the material. As $\dot{F}$ increases, the elastic component becomes predominant.

The simulations have also shown that when a constant tensile force is applied to a CGM comprising amorphous macromolecular chains, the material response depends on the magnitude of the force as well as the time during which it is applied. The magnitude of the force and the time span of force application also affect the extent of viscoelastic recovery after the removal of an applied creep force. However, the rate of recovery exhibits a much smaller dependence on these factors. Previously, the influence of the morphology of the material on its properties had also been demonstrated [51, 52].

These observations are closely related with the competing deformation mechanisms taking place during tensile deformation of the material. The results presented in this paper, particularly sections 4.1, 5.1 and 5.3, confirm that the loading conditions determine the predominant mechanism(s) taking place, as suggested before in [51]. If the deformation is slow, substantial chain unfolding and chain sliding occur. For faster deformation rates, some chain unfolding still takes place, but bond conformation change and bond rupture are quickly observed. In addition, at slower rates the deformation is rather uniform throughout the material, while at faster rates it is more localized. The same conclusion has been reached experimentally for polypropylene by an Austrian–Swiss group [67]. Because of this, fast rates will often lead to fracture near the edges.

At higher creep force values, deformation results mostly from chain separation and crack formation and propagation, with cracks appearing even at relatively low strain values. In contrast, at lower force values, deformation is more homogeneous, resulting mostly from chain unfolding and bond conformation changes. These effects can also be observed in the true stress response, which increases more significantly for higher creep force values. Such

behaviour is due to localized deformation, which reduces the cross-sectional area abruptly in some regions.

True stress calculations have shown how the changes in cross-sectional area result in stress levels much higher than those indicated by the engineering stress. In this way, a more accurate measure of the conditions imposed on the material can be obtained. Moreover, since the material often exhibits highly localized deformation, the true stress in a certain region can increase substantially compared with the average value. In such cases, those regions become probable *loci* for failure to occur.

The influence of the rigid LC second phase on the properties of the material is clearly seen in section 4.3. Although the second phase increases the modulus of the material, thus performing its role as reinforcement, it also reduces the ductility. This effect supports what had been proposed from the results of tensile deformation up to fracture [49]. The loading conditions were found to have a much stronger effect on the properties than the presence of the second phase, at least within the studied range.

Information obtained through computer simulations provides a better understanding of the molecular phenomena that take place during deformation of polymers, giving encouraging property predictions. Nevertheless, the transition from the mesoscale to macroscopic behaviour and properties requires additional work. It is important to note that caution is required when comparing the simulation results presented here with macroscopic properties for two main reasons: (i) the time-scale of MD simulations is several orders of magnitude below that of experimental testing and (ii) the simulations were performed at a mesoscale, not taking into account the formation of supra-molecular structures at the microscale, and considering a small volume of material.

Acknowledgments

Financial support for this research has been provided by the Robert A Welch Foundation, Houston (Grant # B-1203), and by the Fundação para a Ciência e a Tecnologia, Lisbon, through the 3° Quadro Comunitário de Apoio and through the POCTI and FEDER programmes.

References

[1] Brostow W (ed) 2000 *Performance of Plastics* (Munich: Hanser)
[2] Fossey S 2000 *Performance of Plastics* ed W Brostow (Munich: Hanser) p 63
[3] Mavrantzas V G and Theodorou D N 2000 *Macromol. Theory Simul.* **9** 500
[4] Termonia Y and Smith P 1987 *Macromolecules* **20** 835
[5] Termonia Y and Smith P 1988 *Macromolecules* **21** 2184
[6] Termonia Y 1994 *Macromolecules* **27** 7378
[7] Li Y, Ann H and Binienda WK 1998 *Int. J. Solids Struct.* **11** 981
[8] Shbeeb N, Binienda W K and Kreider K 2000 *Int. J. Fract.* **104** 23
[9] Nishioka T 1997 *Int. J. Fract.* **86** 127
[10] Karayiannis N C, Mavrantzas V G and Theodorou D N 2001 *Chem. Eng. Sci.* **56** 2789
[11] Makrodimitris K, Papadopoulos G K and Theodorou D N 2001 *J. Phys. Chem.* B **105** 777
[12] Ayyagari C, Bedrov D and Smith G D 2000 *Macromolecules* **33** 6194
[13] Gerde E and Marder M 2001 *Nature* **413** 285
[14] Fossey S and Tripathy S 1999 *Int. J. Biol. Macromol.* **24** 119
[15] Farmer B L, Chapman B R, Dudis D S and Adams W W 1993 *Polymer* **34** 1588
[16] Qi D, Hinkley J and He G 2005 *Modelling Simul. Mater. Sci. Eng.* **13** 493
[17] Pütz M, Kremer K and Grest G S 2000 *Europhys. Lett.* **49** 735
[18] Kroger M and Hess S 2000 *Phys. Rev. Lett.* **85** 1128
[19] Smith G D, Bedrov D, Li L and Byutner O 2002 *J. Chem. Phys.* **117** 9478
[20] Nuevo M J, Morales J J and Heyes D M 1998 *Phys. Rev.* E **58** 5845

[21] Powles J G and Heyes D M 2000 *Mol. Phys.* **98** 917
[22] Padding J T and Briels W J 2002 *J. Chem. Phys.* **117** 925
[23] Ellero M, Kröger M and Hess S 2002 *J. Non-Newton. Fluid Mech.* **105** 35
[24] Kröger M and Hess S 1993 *Physica* A **195** 336
[25] Tsige M, Soddemann T, Rempe S B, Grest G S, Kress J D, Robbins M O, Sides S W, Stevens M J and Webb III E 2002 *J. Chem. Phys.* **118** 5132
[26] Sides S W, Curro J, Grest G S, Stevens M J, Soddemann T, Habenschuss A and Londono J D 2002 *Macromolecules* **35** 6455
[27] Auhl R, Everaers R, Grest G S, Kremer K and Plimpton S J 2003 *J. Chem. Phys.* **119** 12718
[28] Rottler J and Robbins M O 2001 *Phys. Rev.* E **64** 051801
[29] Rottler J, Barsky S and Robbins M O 2002 *Phys. Rev. Lett.* **89** 148304
[30] Rottler J and Robbins M O 2003 *Phys. Rev.* E **68** 011801
[31] Davies G R 2004 *Modelling Simul. Mater. Sci. Eng.* **12**
[32] Brostow W, D'Souza N A, Kubat J and Maksimov R 1999 *J. Chem. Phys*. **110** 9706
[33] van der Giessen E and Tvergaard V 1994 *Modelling Simul. Mater. Sci. Eng.* **2** 721
[34] Daxner T, Rammerstorfer F G, Segurado J and Pettermann H 2003 *J. Eng. Mater. Technol.* **125** 50
[35] Zhao Q, Nassar R and Hall DE 2001 *J. Press. Vess. Technol.* **123** 373
[36] Hayhurst D R 1994 *Modelling Simul. Mater. Sci. Eng.* **2** 421
[37] McBagonluri-Nuuri D F 1998 *Master's Thesis* Blacksburg: Virginia Polytechnic Institute and State University
[38] Serizawa H, Ando M, Lewinsohn C A and Murakawa H 2001 *Int. J. Mater. Prod. Technol.* **16** 213
[39] Mahadevan S and Mao H 2004 *J. Reinf. Plast. Comp.* **23** 361
[40] Keblinski P, Wolf D and Gleiter H 1998 *Interface Sci.* **6** 208
[41] Samulski E T 1985 *Faraday Disc.* **79** 7
[42] Brostow W *Polymer* **31** 979
[43] Hess M and Lopez B L 1998 *Mechanical and Thermophysical Properties of Polymer Liquid Crystals* ed W Brostow (London: Chapman and Hall) chapter 9
[44] Brostow W and Walasek J 2004 *J. Chem. Phys.* **121** 3272
[45] Akinay A E and Brostow W 2001 *Polymer* **42** 4527
[46] Brostow W and Kubát J 1993 *Phys. Rev.* B **47** 7659
[47] Blonski S, Brostow W and Kubát J 1994 *Phys. Rev.* B **49** 6494
[48] Brostow W, Donahue III M, Karashin C E and Simoes R 2001 *Mater. Res. Innov.* **4** 75
[49] Brostow W, Cunha A M, Quintanilla J and Simoes R 2002 *Macromol. Theory Simul.* **11** 308
[50] Brostow W, Hinze J A and Simoes R 2004 *J. Mater. Res.* **19** 851
[51] Simoes R, Cunha A M and Brostow W 2004 *e-Polymers* no 067
[52] Simoes R, Brostow W and Cunha A M 2004 *Polymer* **45** 7767
[53] Flory P J 1969 *Statistical Mechanics of Chain Molecules* (New York: Wiley)
[54] van Gunsteren W F 1988 *Mathematical Frontiers in Computational Chemical Physics* ed D G Truhlar (New York: Springer)
[55] Alder B J and Wainwright T E 1957 *J. Chem. Phys.* **27** 1208
[56] Rahman A 1964 *Phys. Rev.* **136** A405
[57] Simoes R, Cunha A M and Brostow W 2006 *Comput. Mater. Sci.* **35** at press
[58] Mom V 1981 *J. Comput. Chem.* **2** 446
[59] Brostow W, Cunha A M and Simoes R 2003 *Mater. Res. Innov.* **7** 19
[60] Brostow W, Dziemianowicz T S, Romanski R and Werber W 1988 *Polymer Eng. Sci.* **28** 785
[61] Brostow W and Hess M 1992 *Mater. Res. Soc. Symp.* **255** 57
[62] Brostow W, Cunha A M, Viana J C and Simoes R 2003 *Proc. Ann. Tech. Conf. Soc. Plastics. Engrs.* **61** 2957
[63] Viana J C, Cunha A M and Billon N 1997 *Proc. 10th Int. Conf. on Deformation, Yield and Fracture of Polymers (Cambridge, UK)* (London: Institute of Materials) p 320
[64] Kroger M 2004 *Phys. Rep.* **390** 453
[65] Menard K P 1999 *Dynamic Mechanical Analysis: A Practical Introduction* (Boca Raton: CRC Press)
[66] Menard K P 2000 *Performance of Plastics* ed W Brostow (Munich: Hanser) chapter 8
[67] Grein C, Plummer C J G, Germain Y, Kausch H-H and Beguelin P 2003 *Polymer Eng. Sci.* **43** 223